



A new analytical method based on Co-Mo nanoparticles supported by carbon nanotubes for removal of mercury vapor from the air by the amalgamation of solid-phase air removal

Danial Soleymani-ghoozhdi ^a, Rouhollah Parvari ^a, Yunes Jahani ^b, Morteza Mehdipour-Raboury ^a and Ali Faghihi-Zarandi ^{a,*}

^a Department of Occupational Health and Safety at Work, Kerman University of Medical Sciences, Kerman, Iran

^b Department of Biostatistics and Epidemiology, School of Public Health, Kerman University of Medical Sciences, Kerman, Iran

ARTICLE INFO:

Received 5 Dec 2021

Revised form 10 Feb 2022

Accepted 26 Feb 2022

Available online 28 Mar 2022

Keywords:

Mercury removal,
Air,
Adsorption,
Cobalt and molybdenum nanoparticles,
Multiwalled Carbon nanotube,
Amalgamation solid-phase air removal

ABSTRACT

Heavy metals are a major cause of environmental pollution, and mercury is a well-known toxicant that is extremely harmful to the environment and human health. In this study, new carbon nanotubes coated with cobalt and molybdenum nanoparticles (Co-Mo/MWCNT) were used for Hg⁰ removal from the air by the amalgamation of solid-phase air removal method (ASPAR). In the bench-scale setup, the mercury vapor in air composition was produced by the mercury vapor generation system (HgGS) and restored in a polyethylene airbag (5 Li). In optimized conditions, the mercury vapor in the airbag passed through Co-Mo/MWCNT and was absorbed on it. Then, the mercury was completely desorbed from Co-Mo/MWCNT by increasing temperature up to 220 °C and online determined by cold vapor atomic absorption spectrometry (CV-AAS). The recovery and capacity of Co-Mo/MWCNT were obtained at 98% and 191.3 mg g⁻¹, respectively. The Repeatability of the method was 32 times. The mercury vapors absorbed on Co-Mo/MWCNT adsorbent could be maintained at 7 days at the refrigerator temperature. The Co-Mo/MWCNT as a sorbent has many advantages such as; high capacity, renewable, good repeatability and chemical adsorption (amalgamation) of mercury removal from the air. The method was successfully validated by a mercury preconcentrator analyzer (MCA) and spiking of real samples.

1. Introduction

Heavy metals are a major cause of environmental pollution, and mercury (Hg) is a well-known toxicant that is extremely harmful to the environment and human health because of its persistence, bioaccumulation, and neurological toxicity [1, 2]. Hg can affect many organs and cause a variety of symptoms in the body, although it targets the nervous system, it may also have serious

toxicological effects on the kidney. In addition to the nervous and kidney system, other systems such as the cardiovascular system can also be damaged by exposure to mercury [3, 4]. Mercury has been used in various products and processes due to its unique properties. It is utilized in industrial processes that produce chlorine, sodium hydroxide (Chlor-alkali plants), the vinyl chloride monomer for polyvinyl chloride (PVC) production, and polyurethane elastomers. Mercury is also released from coal-fired power plants and cement production [5, 6]. Therefore, Hg emissions have attracted worldwide attention. Minamata Convention on mercury, which

*Corresponding Author: [Ali Faghihi-Zarandi](mailto:Ali.Faghihi-Zarandi@kmu.ac.ir)

Email: Alifaghihi60@yahoo.com

<https://doi.org/10.24200/amecj.v5.i01.163>

aims is to protect human health and the environment from anthropogenic emissions and releases of mercury and mercury compounds, entered into force on 16 August 2017 [7, 8]. Recently, the different methods have been introduced for the sampling and analysis of mercury. NIOSH 6009 and OSHA 140 are the recommended methods for the sampling of mercury. In these methods, sample preparation depends on the applied nitric acid and hydrochloric acid which can be hazardous to the environment and human health [9, 10]. Emissions from different sources, mercury release in different forms, including elemental mercury (Hg^0), oxidized mercury (Hg^{2+}), and particulate bound mercury (Hg^p) [11, 12]. Among of various states of mercury, Hg^0 is difficult to remove due to its stability, long persistence time, high volatility and insolubility in water [13, 14]. Therefore, effective Hg^0 control technologies are immediately needed. Several control technologies for Hg^0 , including catalytic oxidation [15], photocatalytic oxidation [16], photochemical removal [17], wet oxidation [18], and adsorption method [19] have been developed. Among the various Hg^0 removal methods, the adsorption technique has been widely studied because of its simplicity, economical, and good removing efficiency [20, 21]. In recent years, novel carbon-based materials, such as graphene and graphene oxide, carbon nanotubes and nanofibers, carbon spheres, and metal-organic frameworks, have been applied for Hg^0 removal. Carbon nanotubes (CNTs) are one type of one-dimensional nanomaterials, which have been used for Hg^0 removal from water and air due to their unique physicochemical properties. Carbon-based materials Because of their large surface area, flexible surface chemistry, and variety diversity, are the most widely studied adsorbents for Hg^0 removal from flue gases and air [21–23]. Because of its high removal efficiency, the activated carbon (AC) based adsorption process is considered one of the most effective technologies for mercury removal, but high operation costs and adsorbent loss have impeded its further development [22, 23]. Therefore, developing more cost-effective carbon-based sorbents for Hg^0

removal has significance [21]. In recent years, novel carbon-based materials, such as bio-chars [24], graphene and graphene oxide [25, 26], carbon nanotubes and nanofibers [27, 28], metal-organic frameworks [29], have been applied for Hg^0 removal by analytical methods. Carbon nanotubes (CNTs) are one type of one-dimensional nanomaterials which have been used for Hg^0 removal from water and air due to their unique physicochemical properties [30–32]. Also, to improve the performance of Hg^0 adsorption, some modification methods have been studied which mainly improve the surface pore structure of adsorbents and/or increase the active sites on the surface of adsorbents [33]. Metal or metal oxide loaded on the surface of CNTs and other carbon-based materials were a type of catalyst with both high adsorption and catalytic capability. Consequently, these types of catalysts can be an effective material for Hg^0 removal from the air. Shen et al. reported that the surface area (BET) of activated carbon (AC) was decreased after loading of Mn or Co on AC, but the on the other hand, the metal oxide functionalized on the AC surface can promote Hg^0 catalytic oxidation [34]. Ma et al used the analytical method based on Fe-Ce decorated multi-walled carbon nanotube (MWCNT) for removal of Hg^0 from flue gas. The results showed that Fe-Ce/MWCNT had good Hg^0 removal performance [32]. Liu et al Suggested the adsorption of Co/TiO₂ for Hg^0 . The results showed that the high oxidation activities for Hg^0 was obtained by this catalyst [35]. Molybdenum (Mo) is commonly added as a promoter to vanadium-based catalysts in Hg^0 oxidation, but its catalytic oxidation activity is poor [36].

In this work, Hg^0 was removed from the air by using Co-Mo/MWCNTs. Brunauer–Emmett–Teller (BET) analysis, X-ray diffraction (XRD), scanning electron microscopy (SEM) and transmission electron microscopy (TEM) were employed to analyze the characteristics of the samples. Experimental parameters affecting the Hg^0 removal process from the air such as temperature and flow rate were investigated and optimized. Also, comparisons between the proposed method and previous methods were obtained.

2. Experimental

2.1. Materials and Chemical reagents

Mercury standard was used in the mercury vapor generation system (HgGS). It was prepared by dilution of 1 ppm (1000 mg L⁻¹) Hg (II) standard solution (CAS Number.: 7487-94-7) which was purchased from Fluka, Germany. Deionized water (DW) was prepared by water purification system from RIPI. The stannous chloride (SnCl₂, CAS Number: 7772-99-8) and the NaBH₄ (CAS Number: 6940-66-2) analytical grade were purchased from Merck and Sigma (Germany) which was diluted with DW. The SnCl₂ or the NaBH₄ as reducing agents was used by dissolving in HCl and NaOH/DW, respectively. The reducing agents was added to 100 mL deionized water (DW) and mixed well. All the laboratory glassware (Sigma) and PVC plastics were cleaned by nitric acid (10% v/v) for at least 2 days and then washed for many times with DW. Cobalt (II) nitrate hexahydrate (Co (NO₃)₂.6 H₂O; CAS Number: 10026-22-9) and Molybdenum powder (10 μm, ≥99.95%, CAS Number: 7439-98-7) were purchased from Sigma Aldrich (Germany). The MWCNTs and Co/Mo-MWCNTs adsorbents was synthesized and prepared from nano center of RIPI. In this study, the Co-Mo/MWCNTs adsorbent was used for mercury removal from air.

2.2. Apparatus

The mercury standard (Hg⁰) was generated by the mercury vapor generation system (HgGS) in chamber. The bench scale included of HgGS for HgH₂, chamber, PVC bags, the quartz tubes as a column, the heater accessory (220 AC Voltage, 35-450 °C), the digital flow meter control (50-500 ml min Ar/air), Pure air accessory, O₂ and water digital detectors, the digital temperature control, the MC-3000 as trace mercury analyser (Germany), and the CV-AAS for determining the mercury concentration. The pure air pushed with flowrate of 50-250 ml min⁻¹ to chamber and mixed with mercury vapour at 100 °C. The air lines (tubes) and PVC bags were covered with heating jackets. The quartz tubes with outer diameter of 0.35 inch,

inner diameter of 0.2 inch and length of 4.0 inch was used as a column for the Co-Mo/MWCNTs adsorbent. The Hg⁰ determined by a cold vapor atomic absorption spectrometer (CV-AAS, GBC Plus 932, AUS). A mercury hollow-cathode lamp with a current of 8 mA, the wavelength of 253.7 nm based on a spectral band width (0.5 nm) was used. Argon (99.99%) was used as a carrier gas for mixer of CV-AAS and glass separator. The SKC air sampling pump (USA), 50 to 2000 ml min⁻¹ was used.

2.3. Co and Mo Catalyst preparation

The sol-gel method has been extensively used in the preparation of supported metal catalysts because it typically results in highly homogeneous materials with high degree of metal dispersion. In this sense, catalysts were supported on silica sol-gel with the metal to 50 percent based on silica added. To obtain metallic catalyst supported on high-surface area silica by the sol-gel method, the polymerization of an alkoxy-silane such as tetrathoxysilane (TEOS), also known as tetraethyl orthosilicate, is carried out in the presence of the appropriate metal precursors. In our case, catalyst nanoparticles were prepared from high purity salts of the transition metals: Co (NO₃)₂.6H₂O and (NH₄)₆Mo₇O₄. 4H₂O, from Baker Co. To accelerate the polymerization, an increase in pH can be brought about by addition of a base, which causes a rapid hydrolysis followed by polymerization. Simultaneously with this polymerization process, the metallic ions (Co and Mo) precipitate, thus forming a homogeneous and well-dispersed mixture (Fig.1).

2.4. Co-Mo/MWCNTs synthesis

As Figure 1, After placing the catalyst inside a quartz tube, a continuous nitrogen flow rate of 1 L min⁻¹ was passed through the reactor for removing the oxygen. Subsequently, the reduction process was accomplished within at 600 °C. The reduction process was kept for 30 minutes in an atmosphere of 90 % v/v of N₂ and 10 % v/v of H₂. Next, the temperature was increased up to 700 °C for the nucleation and growing of CNTs [37-39].

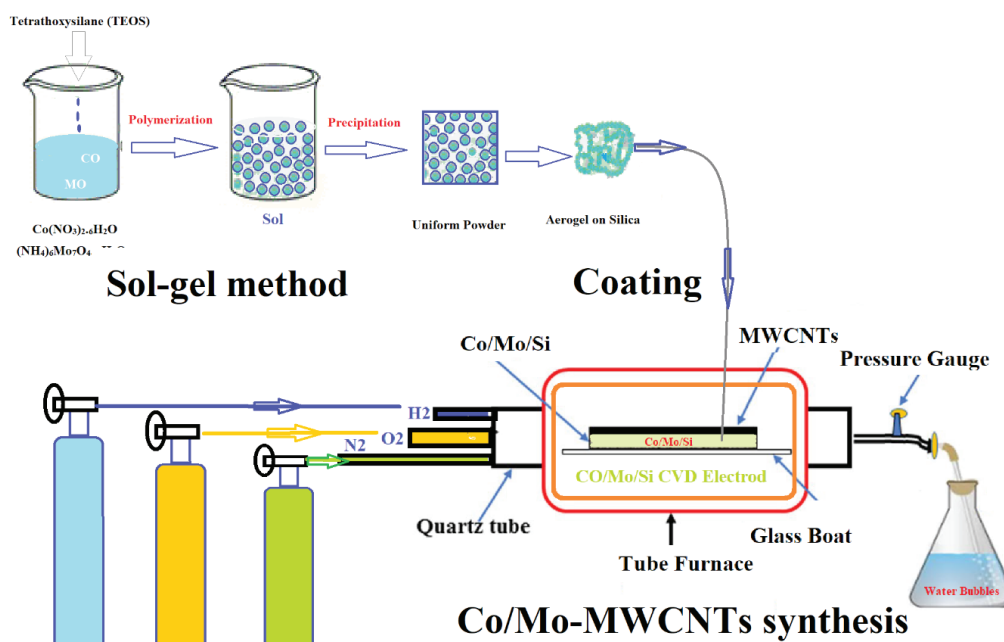


Fig.1. Synthesis of Co-Mo/MWCNTs by Sol gel method and CVD procedure

2.5. Characterization

The high-resolution images were obtained using a high-resolution transmission electron microscope JEOL JEM-2010, operated at 200 kV and a scanning electron microscopy (SEM) JEOL JSM 5300 operated at 5 kV. Complementary RAMAN spectroscopy was performed. The Co-Mo/MWCNTs samples were deposited onto a sample holder with an adhesive carbon foil and sputtered with Au before imaging. The morphology of Co-Mo/MWCNTs was obtained by a transmission electron microscopy (TEM, Zeiss, Germany). For the TEM analysis, the samples were dispersed in C_2H_5OH and a drop was used. The chemical analysis for the determination of Co and Mo concentration in synthesized samples was performed using F-AAS.

2.6. General Procedure

The mercury vapor removal was performed using a bench-scale setup (Fig. 2). First, 40 mg of Co-Mo/MWCNTs nanoadsorbent was put onto the quartz tubes. Then, the end of the adsorbent were tied by fire-proof linen. The pure air was mixed with mercury vapor in chamber containing $0.1-10 \mu\text{g Hg}^0$ per liter air (21% O_2 , 0.2% H_2O) at 25°C .

By the procedure, $0.1-10 \mu\text{g}$ of Hg^0 was generated by the mercury vapor generation system (HgGS) and restored in a PVC bag. The value of mercury in PVC bag was validated using MC analyzer. Due to procedure, the mercury standard solution ($1-2 \text{ mL min}^{-1}$), HCl (5% v/v, 5 mL min^{-1}), and $SnCl_2$ as reducing agent (2.5 mL min^{-1}) were mixed with pure air in mixer and pass through a peristaltic pumps. Elemental mercury vapor was generated in the reaction loop, and pumped into a 5 L polyethylene (PE) bag, as a bulk container. Finally, the mercury concentration was obtained $0.1-10 \mu\text{g Hg}^0$ per liter air in the polyethylene bag (5 L) was mixed with 21 % O_2 and 0.2 % H_2O vapor at 25°C ($10-100 \times \text{TLV OSHA}$). Then The mixture Hg^0 and pure air passed through 40 mg of the Co-Mo/MWCNTs adsorbents, at optimized air flow rate 250 ml min . After amalgamation/adsorption process, the elemental mercury was released from the Co-Mo/MWCNTs adsorbents by a thermal desorption accessory at 220°C , under Ar flow rate and transferred to the absorption cell of CV-AAS (Fig.2). Finally, Hg^0 concentration was determined by CV-AAS. The conditions were presented in Table 1.

3. Results and Discussion

3.1. Co-Mo/MWCNTs Raman Spectra

Figure 3a shows the Raman spectra for CNTs-Co, in which the ratio ID/IG is 0.26, relating a high purity material. On the other hand, with Mo the quality is decreased in a high level (Figure 3b), mainly with Mo (ID/IG ~ 0.59). This is due to the solubility of C in Mo. In order to obtain a better quality, in this case the CVD process must be performed to high temperatures (~900°C). In our experiments, for comparison purposes, the temperature was always the same for the different metal-catalyst (~700°C). According

to previous reports, the increase of the D band intensity (characteristic peak at ~1350 cm⁻¹) with decreasing multiwalled carbon nanotubes (MWCNT) content, is a direct result of the addition of carbonaceous by-products. In the same sense, a decrease in the G' band intensity (characteristic peak at ~2700 cm⁻¹) is observed as the MWCNT mass fraction decreases. The G' band on Figures a reflects the well-structured carbon walls in the samples with Co catalyst, while the Figure 3b (CNTs-Mo), indicate a less ordered structures, due to the carbonaceous byproducts.

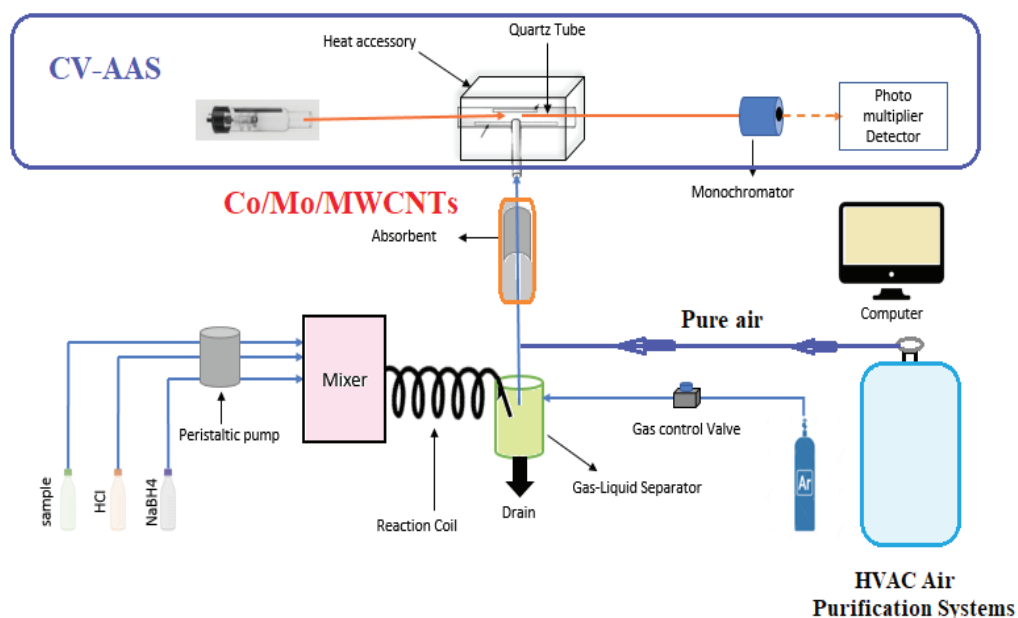


Fig.2. The procedure for removal mercury vapor from air based on Co-Mo/MWCNTs by the ASPAR procedure

Table1. Method conditions for mercury vapor removal with the Co-Mo/MWCNTs

Chamber Conditions	Value
Hg ⁰ values	0.1–10 µg per liter
O ₂ (g)	21%
H ₂ O (g)	0.2%
PVC bag	5 L
Ar flow rate	0.2 L min ⁻¹
Air flowrate	0.25 L min ⁻¹
Heat	220 °C
Removal efficiency with air	More than 95%
Absorption capacity	191.3 mg g ⁻¹ (2% Co and 2% Mo)
Adsorbent amount	40 mg

3.2. SEM imaging

The morphology and structural features of Co-Mo/MWCNTs and MWCNTs were shown by the SEM images. As shown in Figures 4a and 4b, the morphology of MWCNTs and the Co-Mo/MWCNTs

were shown in the nanoscale range between 30–80 nm. Co and Mo were seen in MWCNTs as the brilliant spots. The elemental analysis (EDX) of Co-Mo/MWCNTs was shown in Table 2.

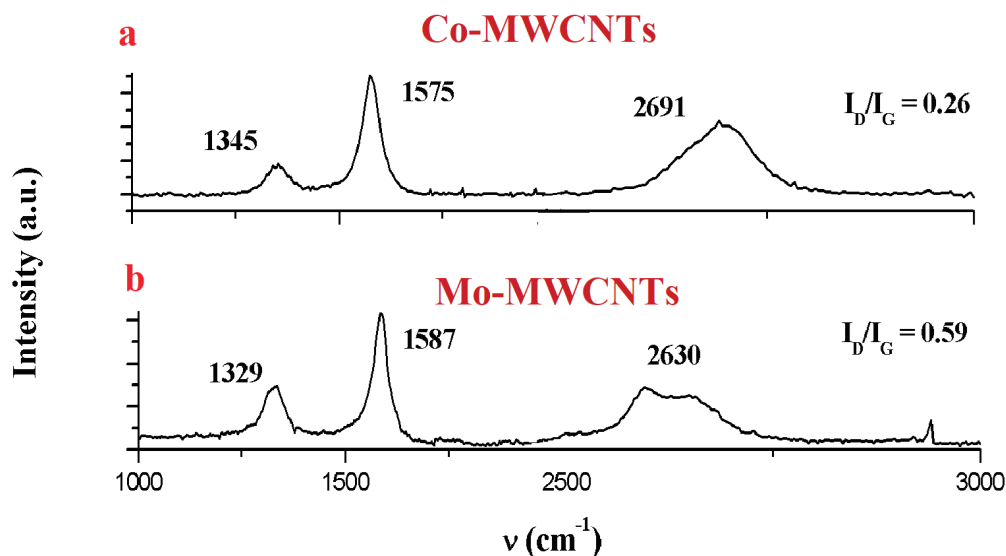


Fig.3. Raman spectra of CNTs samples using a) Co-MWCNTs and b) Mo-MWCNTs

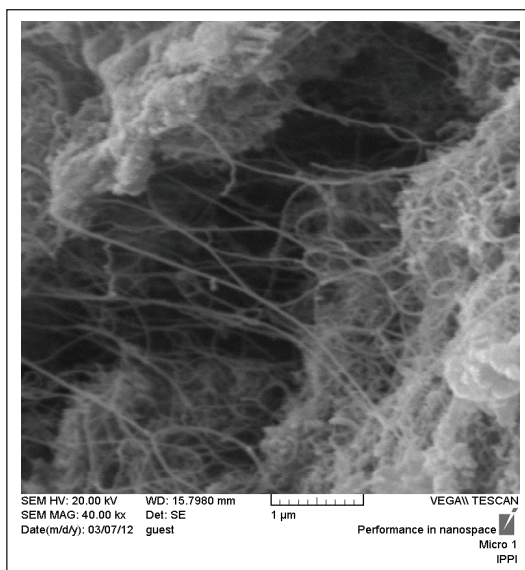


Fig.4a. SEM image of MWCNTs

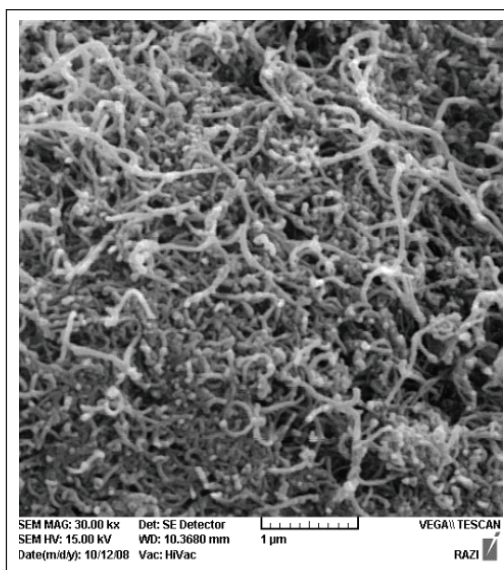


Fig.4b. SEM image of Co-Mo/MWCNTs

Table 2. EDX analysis for elemental values for the Co-Mo/MWCNTs

Elements	% Values
Carbon	67.5
N	17.2
Co	2.6
Mo	2.8
H	4.3
O	5.6

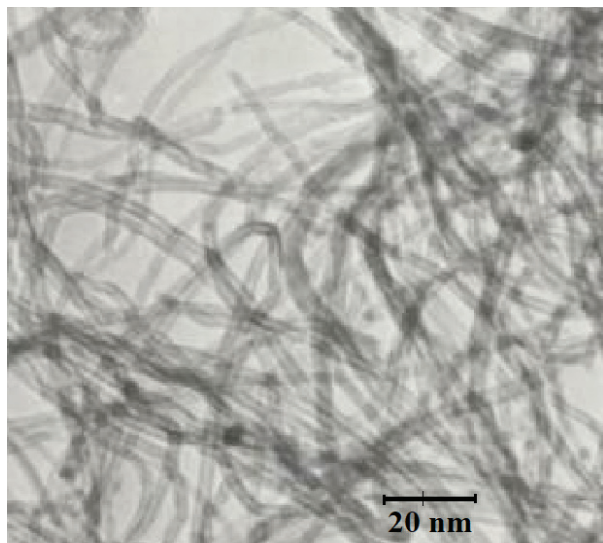


Fig. 5a. TEM image of MWCNTs



Fig. 5b. TEM image of Co-Mo/MWCNTs

3.3. TEM imaging

The TEM of MWCNTs showed in [Figure 5a](#). Also. The TEM of Co-Mo/MWCNTs adsorbent can be seen that Co and Mo nanoparticles (brilliant points) were incorporated into the MWCNTs, both on the external and internal surface of MWCNTs, with no effect on the porous structure of MWCNTs ([Fig. 5b](#)). The Co and Mo particles in MWCNTs distributed with the average size of 35 nm (20-50 nm).

3.4. XRD analysis

The immobilized Co and Mo on MWCNTs were characterized by XRD spectroscopy. In [Figure](#)

[6](#). A many peaks can be observed from Co-Mo/MWCNTs, which was ascribed to the highly crystalline structure of carbon nanotubes. The diffraction peaks at 26° and 41° are related to (002) and (100) planes of hexagonal graphite. There are, however, no characteristic peaks of Co and Mo in the XRD pattern of Co/Mo-MWCNTs. This indicates that Co and Mo are uniform dispersed on the MWCNTs, and no effect on XRD spectrum of MWCNTs. The Textural properties of samples for Co-Mo/MWCNTs and MWCNTs adsorbents synthesized with the CO-MO/MWCNTs ([Table 3](#))

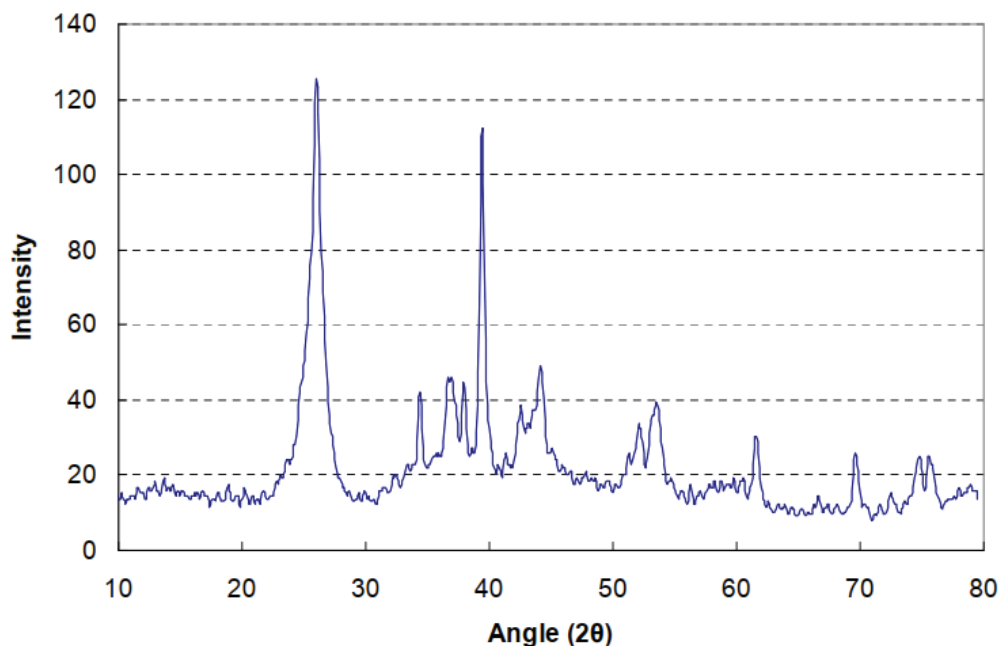


Fig. 6. The XRD analysis for CO/MO-MWCNTs

Table 3. Textural properties of samples synthesized with the Co-Mo/MWCNTs

Material	S_{BET} ($m^2 g^{-1}$) ^a	V ($cm^3 g^{-1}$) ^b	a (nm) ^c	d (nm) ^d	W (nm) ^e
MWCNTs	288.84	0.52	5.1	3.85	1.55
CO-MO/MWCNTs	145.16	0.34	4.9	3.8	1.62

^a BET specific surface area, ^b the pore volume, ^c Unit cell parameter obtained from XRD diffractograms,

^d the pore diameter (nm), ^e Wall thickness(nm)

3.5. Optimization of parameters for removal mercury

In this work, a novel method was used for the removal of mercury vapor (Hg^0) from air by using of the Co-Mo/MWCNTs adsorbent. The chamber was designed to generate a gas containing amounts of mercury vapor based on O_2 and H_2O vapor. For efficient removal of Hg^0 , the conditions of proposed method were optimized.

3.5.1. Effect of O_2 and H_2O

The general procedure was performed with O_2 and H_2O vapor for Hg^0 removal by Co-Mo/MWCNTs adsorbent. In presence of O_2 and H_2O vapor, the percentages of mercury removal decreased about 4-8%. Due to oxidation of the Co-Mo/MWCNTs, the surface activity of the adsorbent decreased. The results showed, the quantitative recoveries of Hg^0 were obtained at the moisture contents of 0.05-0.22%. By increasing of water vapor content, slightly decreased the recovery values. By increasing the O_2 , the surface morphology of the Co-Mo/MWCNTs adsorbent was changed due to the oxidation of Co and Mo nanoparticles. So, the removal efficiency of adsorbent a slightly decreased at 25°C (5%). On the other hand, the oxidation process accelerates in high temperature and reduce the surface area (BET) and the adsorption capacity. At 35-55 °C, the removal efficiency was decreased from 5% to 25% in present of O_2 value.

3.5.2. Effects of Co-Mo/MWCNTs amount and flow rate

The effect of the Co-Mo/MWCNTs amount on the mercury removal from air was evaluated (Fig. 7). It was evaluated with different amounts of Co-Mo/MWCNTs adsorbent in

the range of 1 to 50 mg. Due to results, the adsorption of Hg^0 was increased more than 25 mg of adsorbent. So, the high recovery for removal of mercury vapor in air were achieved more than 95% by 40 mg of Co-Mo/MWCNTs adsorbent. Also, the MWCNTs adsorbent had low recovery about 10-14%. Due to high surface area and metal sites of Co and Mo, the high absorption capacity was achieved for the Co-Mo/MWCNTs adsorbent by amalgamation process (Co-Hg; Mo-Hg).

The mercury vapor was generated in chamber and mixed with pure air (21% O_2 ; 0.2% of H_2O , 0.1-10 $\mu g L^{-1}$). The flow rate is a critical role in removal recovery of mercury, which was directly affected on interaction and adsorption process. The flow rate must be tuned to enable a high recovery for mercury removal from air. So, the effect of flow rates was evaluated in ranges of 50-500 $mL min^{-1}$ (25°C). The results showed us, the best removal efficiency was occurred at flow rates of 50-300 $mL min^{-1}$ (25°C). However, it was observed that the absorption process started to decrease at more than 300 mL

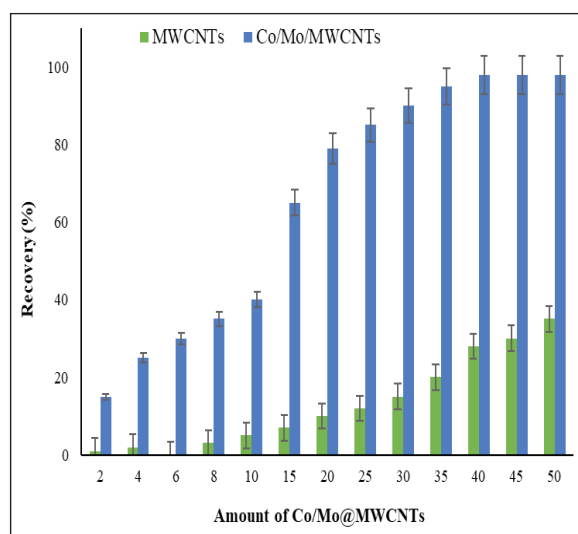


Fig. 7. The effect of sorbent mass for Hg^0 removal

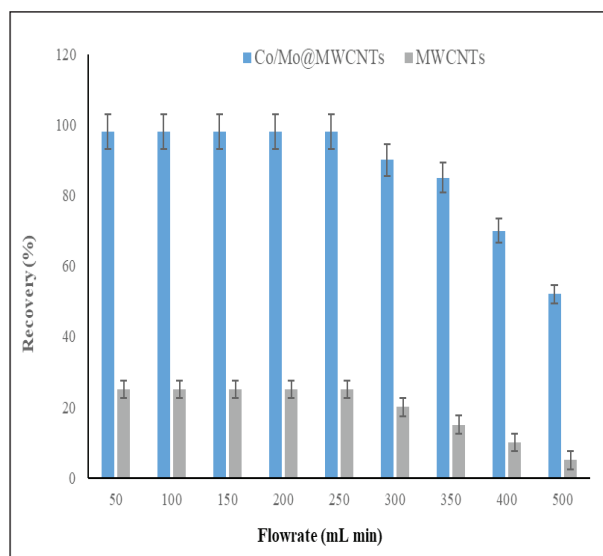


Fig. 8. The effect of flowrate for Hg⁰ removal

min⁻¹. Therefore, the flowrate of 250 mL min⁻¹ was selected as optimum flowrate for mercury removal by the Co-Mo/MWCNTs adsorbent (Fig. 8).

3.5.3. Effect of temperature

The main role for the adsorption and desorption of Hg⁰ by the Co-Mo/MWCNTs and MWCNTs adsorbents is temperature. So, the effect of temperature for the adsorption and desorption of mercury from Co-Mo/MWCNTs adsorbents were examined in the range of 25–60°C and 50–400°C, respectively (21% O₂, 0.2% H₂O; 0.1–10 µg L⁻¹ Hg⁰). As Figure 9, the mercury vapor removed from air at temperatures up to 30 °C. In higher temperatures

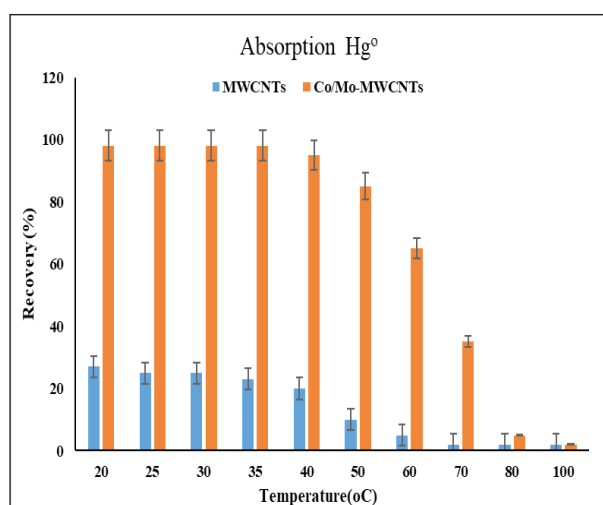


Fig. 9. Effect of temperature on absorption mercury

the Hg⁰ adsorption was decreased. Moreover, the desorption of Hg⁰ from the Co-Mo/MWCNTs and MWCNTs adsorbents were obtained at 190–250 °C. Therefore, the Co-Mo/MWCNTs can be removed the mercury from air by the amalgamation interactions at 220 °C (Fig. 10).

3.5.4. Adsorption capacity

In-addition the adsorption capacities of mercury vapor by the Co-Mo-MWCNTs and MWCNTs adsorbents were evaluated (21% O₂, 0.2% H₂O; 0.1–10 µg L⁻¹ Hg⁰). The mercury vapor was generated and passed through the Co-Mo/MWCNTs and MWCNTs adsorbents (40 mg) at the optimized conditions. The maximum adsorption capacities of the Co-Mo/MWCNTs and MWCNTs adsorbents for mercury removal from air were obtained 191.3 mg g⁻¹ and 22.4 mg g⁻¹, respectively. This mechanism was related to the interaction of mercury with Mo and Co which was supported on MWCNTs due to amalgamation process. The physical adsorption of MWCNTs (about 20%) and chemical adsorption by the amalgamation processes (more than 80%) caused to increase the removal efficiency of mercury from air. In chamber, 40 mg of the Co-Mo/MWCNTs and MWCNTs adsorbents were placed on PVC bag and mercury vapor generated/ flowed in column by 250 mL min⁻¹. Then the mercury concentration in stock PVC bag was determined by MC-3000. In dynamic system, the adsorption

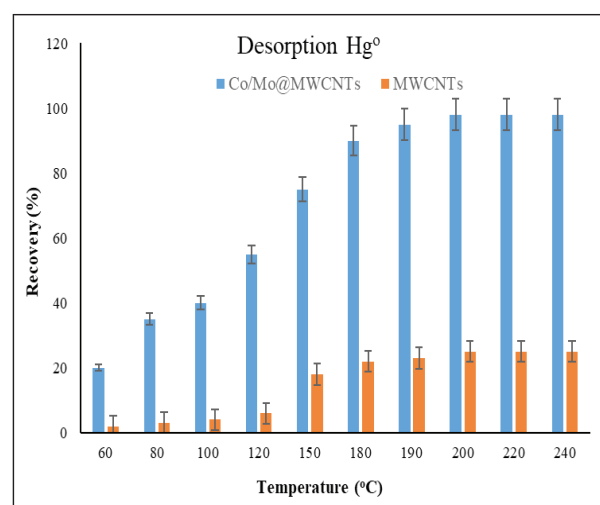


Fig. 10. Effect of temperature on desorption mercury

capacities of the Co-Mo/MWCNTs and MWCNTs for mercury removal were found 132.7 mg g⁻¹ and 8.4 mg g⁻¹, respectively which was lower than static system. The reusability of the Co-Mo/MWCNTs adsorbent for mercury removal was decreased after 32 times absorption/desorption process.

3.5.5. Method Validation

The ASPAR method was used for the removal of Hg⁰ from the air. The method was validated based on the Co-Mo/MWCNTs and MWCNTs adsorbent by spiking real samples in presence of air (21% O₂, 0.2% H₂O; 0.1-10 µg L⁻¹ Hg⁰). Due to absorption and desorption process the concentration of mercury was determined by CV-AAS at optimized conditions. Also, the validation of the methodology was followed by MC3000

analyzer. There is no standard reference material (SRM) for mercury vapor from air, So, the method validation for Hg⁰ removal found by spiking of the standard mercury solutions which was confirmed the accuracy and precision of the ASPAR method. The mixture of mercury in pure air (21% O₂, 0.2% H₂O, 0.1-10 µg), was moved from chamber to the PVC bags and then moved into the Co-Mo/MWCNTs and MWCNTs adsorbents. Many spiked samples based on various concentration of Hg⁰ were used in presence of air (Table 4). The procedure was found for real samples in presence of air composition which was validated based on spiking samples and compared to MC3000 analyzer (Table 5). The results showed a simple, low cost, high recovery and favorite repeatability for mercury removal from air.

Table 4. Validation of the ASPAR method based on Co-Mo/MWCNTs by spiking of mercury vapour (µg L⁻¹ air)

Sample	**HgGS	Added	*Found	Recovery (%)
Air 1	0.102± 0.005	-----	0.108± 0.006	-----
		0.1	0.210± 0.011	102
Air 2	0.532± 0.026	-----	0.528± 0.025	-----
		0.5	1.021± 0.044	98.6
Air 3	1.076± 0.062	-----	1.009± 0.066	-----
		1.0	1.984± 0.096	97.5
Air 4	3.035± 0.145	-----	2.965± 0.152	-----
		3.0	5.882± 0.274	97.2
Air 5	5.578± 0.238	-----	5.397± 0.255	-----
		5.0	10.226± 0.513	96.6
Air 6	10.124± 0.453	-----	9.965± 0.493	-----
		10	20.051± 0.937	100.9

*Mean of three determinations ± confidence interval (P = 0.95, n = 3)

** Mercury in HgGS determined by CV-AAS (n=10)

Table 5. Validation of the ASPAR method based on Co-Mo/MWCNTs by spiking of real sample and compared to MCA (µg L⁻¹ air)

Sample	**MCA(µg)	Added (µg)	*Found (µg)	Recovery (%)
Air I	0.402± 0.018	-----	0.392± 0.022	97.5
		0.5	0.882± 0.042	98.0
Air II	0.957± 0.053	-----	0.962± 0.063	100.5
		1.0	1.938± 0.096	97.6
Air III	2.882± 0.144	-----	2.756± 0.154	95.6
		2.5	5.198± 0.268	97.7
Air VI	5.264± 0.246	-----	5.361± 0.253	101.8
		5.0	10.188± 0.483	96.5
Air V	8.016± 0.412	-----	7.914± 0.388	98.7
		10	17.865± 0.832	99.5

*Mean of three determinations ± confidence interval (P = 0.95, n = 3)

**Mercury determined by MC3000

3.5.6. Discussion

By the ASPAR method, the mercury removal from air was achieved based on Co-Mo/MWCNTs adsorbent and compared to other published methods (Table 6). Ma et al were investigated on Hg⁰ removal by multi-walled carbon nanotubes supported Fe-Ce mixed oxides nanoparticles (Fe-CeO_x/MWCNTs). The Fe₍₂₎ Ce_(0.5) O_x/MWCNTs catalyst showed the best catalytic activity, its Hg⁰ removal efficiency reached as high as 88.9% at 240 °C [32]. Also, the removal of Hg⁰ was studied based on Mn-Mo/CNT by Zhao et al. The optimum temperature and MnO₂ content for removal of Hg⁰ was 250 °C and 5 wt%. Also, experimental of mercury oxidized by Mn-Mo/CNT indicated that SO₂ could increase mercury oxidation by this catalyst and that the optimum temperature for mercury oxidized by Mn-Mo/CNT decreased to 150 °C [27]. According to the study of Wu et al, the removal efficiency of Hg⁰ based on Ce-Mn/TiO₂ was investigated by N₂, 6% O₂ and 500–2000 ppm of SO₂. The average removal efficiency of Ce-Mn/TiO₂ was obtained about 80% which was lower than Co-Mo/MWCNTs (more than 95%). Furthermore, the results showed the reusability of Ce-Mn/TiO₂ was achieved for 10 times (adsorption/desorption cycles) which was

lower than the Co-Mo/MWCNTs adsorbent with 32 times [2]. Ma et al showed the Hg⁰ removal from flue gas with Ag-Fe₃O₄@rGO composite. The Hg⁰ was efficiently removed higher than 92% at 100 °C, which was lower than Co-Mo/MWCNTs [26]. Yang et al was studied on Hg⁰ removal from air based on Fe_{3-x}Mn_xO₄/CNF. The results showed that at the optimal temperature (150–200 °C), the removal efficiency for Hg⁰ was attained above 90 % [28]. Xu et al showed that ultrasound-assisted impregnation promoted Hg⁰ removal with Cu-Ce/RSU. the optimal Cu/Ce molar ratio, loading value and reaction temperature were 1/5, 0.18 mol L⁻¹ and 150 °C, respectively. Also, the highest Hg⁰ removal efficiency obtained was 95.26%. As compared to Co-Mo/MWCNTs, the removal efficiency of Cu-Ce/RSU was lower value [24]. In another study, Xu et al synthesized MnO_x/graphene composites for the removal of Hg⁰ in flue gas. MnO_x/graphene sorbents with 30% graphene showed that the Hg⁰ removal efficiency was achieved more than 90% at 150 °C (4% O₂). Furthermore, MnO_x/graphene showed a good regenerative ability [25]. Liu et al. prepared Co/TiO₂ catalysts for Hg⁰ removal. results showed that the optimal loading of Co was 7.5%. The Hg⁰ removal efficiency was reached more than 90% at the temperature range 120–330 °C [35].

Table 6. Comparing of ASPAR method for the mercury removal from air based on Co-Mo/MWCNTs with other published methods

Adsorbent	Mechanism/method	Sample	Adsorption capacity	Removal Efficiency	Ref.
Mn-Mo/CNT	chemisorption	Flue gas	--	80%	[27]
Ag-CNT	Amalgamation	Flue gases	9.3 mg g ⁻¹	---	[40]
Silver nano particles/MGBs	Amalgamation/SPGE	Air/Artificial Air	91.8 mg g ⁻¹	98%	[41]
NPd@MSN	amalgamation/adsorption	Air	149.4 mg g ⁻¹	95%	[42]
Mn/MCM-22	catalytic oxidation and chemisorption	Flue gas	300 mg g ⁻¹	92%	[43]
Cu-Zn/SBA-15	Adsorption	Natural Gas	12.75 mg g ⁻¹	100%	[44]
Co-Mo/MWCNTs	Amalgamation	Air	191.3 mg g ⁻¹	98%	This study

4. Conclusions

In this research, a novel Co-Mo/MWCNTs adsorbent was used for mercury removal from air by the ASPAR method and finally mercury was measured by CV-AAS. First the mercury vapor generated by HgGS (0.1-10 $\mu\text{g L}^{-1}$ air), mixed with pure air (21% of O_2 and 0.2% of H_2O) and moved to column which was filled with the Co-Mo/MWCNTs adsorbent. The mechanism of absorption was obtained by amalgamation Co and Mo. The best thermal desorption was occurred at 220 °C. Due to results, the mean recovery, the reusing and adsorption capacity were obtained 98.8%, 32, 191.3 mg g^{-1} , respectively. The range of adsorption efficiencies for ten air samples with 40 mg of the Co-Mo/MWCNTs adsorbent was achieved between 94.6-102.4 in optimized conditions. The O_2 content may be affected by oxidation of Co or Mo and can reduce the mercury adsorption by the adsorbent by about 5-10%. The ASPAR method was validated by spiking samples and MC3000 analyzer.

5. Acknowledgements

The authors thanks from department of occupational health and safety at work and department of biostatistics and epidemiology, Kerman University of Medical Sciences (KUMS), Kerman, Iran.

6. References

- [1] H. Wang, S. Wang, Y. Duan, Y.-n. Li, Y. Xue, Z. Ying, Activated carbon for capturing Hg in flue gas under O_2/CO_2 combustion conditions. Part 1: Experimental and kinetic study, *Energy Fuels*, 32 (2018) 1900-1906. <https://doi.org/10.1021/acs.energyfuels.7b03380>.
- [2] X. Wu, Y. Duan, N. Li, P. Hu, T. Yao, J. Meng, S. Ren, H. Wei, Regenerable Ce-Mn/ TiO_2 catalytic sorbent for mercury removal with high resistance to SO_2 , *Energy Fuels*, 33 (2019) 8835-8842. <https://doi.org/10.1021/acs.energyfuels.9b00978>.
- [3] G. Genchi, M.S. Sinicropi, A. Carocci, G. Lauria, A. Catalano, Mercury exposure and heart diseases, *Int. J. Environ. Res. Public Health*, 14 (2017) 74. <https://doi.org/10.3390/ijerph14010074>.
- [4] S.E. Orr, C.C. Bridges, Chronic kidney disease and exposure to nephrotoxic metals, *Int. J. Mol. Sci.*, 18 (2017) 1039. <https://doi.org/10.3390/ijms18051039>.
- [5] E.G. Pacyna, J.M. Pacyna, F. Steenhuisen, S. Wilson, Global anthropogenic mercury emission inventory for 2000, *Atmos. Environ.*, 40 (2006) 4048-4063. <https://doi.org/10.1016/j.atmosenv.2006.03.041>.
- [6] C. Winder, N.H. Stacey, Occupational toxicology, 2ed, CRCpress, 2004. <https://www.routledge.com/Occupational-Toxicology/Winder-Stacey/p/book/9780367394554>
- [7] M. Sakamoto, N. Tatsuta, K. Izumo, P.T. Phan, L.D. Vu, M. Yamamoto, M. Nakamura, K. Nakai, K. Murata, Health impacts and biomarkers of prenatal exposure to methylmercury: Lessons from Minamata, Japan, *Toxins*, 6 (2018). <https://doi.org/10.3390/toxins6030045>.
- [8] UNEP, Minamata convention on mercury, United Nations environment programme Geneva, Switzerland, 2013. <https://www.unep.org/resources/report/minamata-convention-mercury>.
- [9] R. Andrews, P.F. O'Connor, NIOSH manual of analytical methods (NMAM), 2020. <https://www.cdc.gov/niosh/nmam/default.html>.
- [10] A. Ebrahimi, A. Salarifar, Air pollution Analysis: Nickel paste on Multi-walled carbon nanotubes as a novel adsorbent for the mercury removal from air, *Anal. methods. Environ. chem. J.*, 2 (2019) 79-88. <https://doi.org/10.24200/amecj.v2.i03.70>.
- [11] Y. Liu, Y. Li, H. Xu, J. Xu, Oxidation removal of gaseous Hg^0 using enhanced-Fenton system in a bubble column reactor, *Fuel*, 246 (2019) 358-364. <https://doi.org/10.1016/j.fuel.2019.03.018>.
- [12] S. Zhang, M. Díaz-Somoano, Y. Zhao, J. Yang, J. Zhang, Research on the mechanism of elemental mercury removal over Mn-Based SCR catalysts by a developed Hg-TPD method, *Energy Fuels*, 33 (2019) 2467-2476. <https://doi.org/10.1021/acs.energyfuels.8b04424>.

- [13] H. Zeng, F. Jin, J. Guo, Removal of elemental mercury from coal combustion flue gas by chloride-impregnated activated carbon, *Fuel*, 83 (2004) 143-146. [https://doi.org/10.1016/S0016-2361\(03\)00235-7](https://doi.org/10.1016/S0016-2361(03)00235-7).
- [14] B. Zhang, P. Xu, Y. Qiu, Q. Yu, J. Ma, H. Wu, G. Luo, M. Xu, H. Yao, Increasing oxygen functional groups of activated carbon with non-thermal plasma to enhance mercury removal efficiency for flue gases, *Chem. Eng. J.*, 263 (2015) 1-8. <https://doi.org/10.1016/j.cej.2014.10.090>.
- [15] H. Li, S. Wu, C.Y. Wu, J. Wang, L. Li, K. Shih, SCR atmosphere induced reduction of oxidized mercury over CuO-CeO₂/TiO₂ catalyst, *Environ. Sci. Technol.*, 49 (2015) 7373-7379. <https://doi.org/10.1021/acs.est.5b01104>.
- [16] J. Wu, C. Li, X. Zhao, Q. Wu, X. Qi, X. Chen, T. Hu, Y. Cao, Photocatalytic oxidation of gas-phase Hg⁰ by CuO/TiO₂, *App. Catal. B*, 176-177 (2015) 559-569. <https://doi.org/10.1016/j.apcatb.2015.04.044>.
- [17] Y. Liu, J. Zhang, J. Pan, Photochemical oxidation removal of Hg⁰ from flue gas Containing SO₂/NO by an ultraviolet irradiation/hydrogen peroxide (UV/H₂O₂) process, *Energy Fuels*, 28 (2014) 2135-2143. <https://doi.org/10.1021/ef401697y>.
- [18] Y. Liu, Y. Wang, Gaseous elemental mercury removal using VUV and heat coactivation of Oxone/H₂O/O₂ in a VUV-spraying reactor, *Fuel*, 243 (2019) 352-361. <https://doi.org/10.1016/j.fuel.2019.01.130>.
- [19] D. Liu, W. Zhou, J. Wu, Kinetic behavior of elemental mercury sorption on cerium- and lanthanum-based composite oxides, *Surf. Rev. Lett.*, 26 (2019) 1-9. <http://dx.doi.org/10.1142/S0218625X1850141X>.
- [20] G. Li, Q. Wu, S. Wang, Z. Li, H. Liang, Y. Tang, M. Zhao, L. Chen, K. Liu, F. Wang, The influence of flue gas components and activated carbon injection on mercury capture of municipal solid waste incineration in China, *Chem. Eng. J.*, 326 (2017) 561-569. <https://doi.org/10.1016/j.cej.2017.05.099>.
- [21] H. Yang, Z. Xu, M. Fan, A.E. Bland, R.R. Judkins, Adsorbents for capturing mercury in coal-fired boiler flue gas, *J. Hazard. Mater.*, 146 (2007) 1-11. <https://doi.org/10.1016/j.jhazmat.2007.04.113>.
- [22] Z. Tan, L. Sun, J. Xiang, H. Zeng, Z. Liu, S. Hu, J. Qiu, Gas-phase elemental mercury removal by novel carbon-based sorbents, *Carbon*, 50 (2012) 362-371. <https://doi.org/10.1016/j.carbon.2011.08.036>.
- [23] Y. Zheng, A.D. Jensen, C. Windelin, F. Jensen, Dynamic measurement of mercury adsorption and oxidation on activated carbon in simulated cement kiln flue gas, *Fuel*, 93 (2012) 649-657. <https://doi.org/10.1016/j.fuel.2011.09.053>.
- [24] W. Xu, Y.G. Adewuyi, Y. Liu, Y. Wang, Removal of elemental mercury from flue gas using CuOx and CeO₂ modified rice straw chars enhanced by ultrasound, *Fuel Proc. Technol.*, 170 (2018) 21-31. <https://doi.org/10.1016/j.fuproc.2017.10.017>.
- [25] H. Xu, Z. Qu, C. Zong, W. Huang, F. Quan, N. Yan, MnOx/graphene for the catalytic oxidation and adsorption of elemental mercury, *Environ. Sci. Technol.*, 49 (2015) 6823-6830. <https://doi.org/10.1021/es505978n>.
- [26] Y. Ma, B. Mu, X. Zhang, H. Xu, Z. Qu, L. Gao, B. Li, J. Tian, Ag-Fe₃O₄@rGO ternary magnetic adsorbent for gaseous elemental mercury removal from coal-fired flue gas, *Fuel*, 239 (2019) 579-586. <https://doi.org/10.1016/j.fuel.2018.11.065>.
- [27] B. Zhao, X. Liu, Z. Zhou, H. Shao, M. Xu, Catalytic oxidation of elemental mercury by Mn-Mo/CNT at low temperature, *Chem. Eng. J.*, 284 (2016) 1233-1241. <https://doi.org/10.1016/j.cej.2015.09.090>.
- [28] J. Yang, Y. Zhao, S. Liang, S. Zhang, S. Ma, H. Li, J. Zhang, C. Zheng, Magnetic iron-manganese binary oxide supported on carbon nanofiber (Fe_{3-x}MnxO₄/CNF) for efficient removal of Hg⁰ from coal combustion flue

- gas, *Chem. Eng. J.*, 334 (2018) 216-224. <https://doi.org/10.1016/j.cej.2017.10.004>.
- [29] X. Zhang, B. Shen, S. Zhu, H. Xu, L. Tian, UiO-66 and its Br-modified derivatives for elemental mercury removal, *J. Hazard. Mater.*, 320 (2016) 556-563. <https://doi.org/10.1016/j.jhazmat.2016.08.039>.
- [30] B. Tawabini, A. A. M. Khaled, Removal of mercury from water by multi-walled carbon nanotubes, *Water Sci. Technol.*, 61 (2010) 591-598. <https://doi.org/10.2166/wst.2010.897>.
- [31] F. Golbabaie, A. Ebrahimi, H. Shir Khanloo, A. Koochpaie, A. Faghihi-Zarandi, Single-walled carbon nanotubes (SWCNTs), as a novel sorbent for determination of mercury in air, *Glob. J. Health Sci.*, 8 (2015) 273. <https://doi.org/10.5539/gjhs.v8n7p273>.
- [32] Y. Ma, D. Zhang, H. Sun, J. Wu, P. Liang, H. Zhang, Fe-Ce mixed oxides supported on carbon nanotubes for simultaneous removal of NO and Hg⁰ in flue gas, *Ind. Eng. Chem. Res.*, 57 (2018) 3187-3194. <https://doi.org/10.1021/acs.iecr.8b00015>.
- [33] W. Xu, A. Hussain, Y. Liu, A review on modification methods of adsorbents for elemental mercury from flue gas, *Chem. Eng. J.*, 346 (2018) 692-711. <https://doi.org/10.1016/j.cej.2018.03.049>.
- [34] Z. Shen, J. Ma, Z. Mei, J. Zhang, Metal chlorides loaded on activated carbon to capture elemental mercury, *J. Environ. Sci.*, 22 (2010) 1814-1819. [https://doi.org/10.1016/S1001-0742\(09\)60324-7](https://doi.org/10.1016/S1001-0742(09)60324-7).
- [35] Y. Liu, Y. Wang, H. Wang, Z. Wu, Catalytic oxidation of gas-phase mercury over Co/TiO₂ catalysts prepared by sol-gel method, *Catal. Commun.*, 12 (2011) 1291-1294. <http://dx.doi.org/10.1016/j.catcom.2011.04.017>.
- [36] S. Zhao, Z. Li, Z. Qu, N. Yan, W. Huang, W. Chen, H. Xu, Co-benefit of Ag and Mo for the catalytic oxidation of elemental mercury, *Fuel*, 158 (2015) 891-897. <https://doi.org/10.1016/j.fuel.2015.05.034>.
- [37] L.C. Klein, Sol-Gel Processing of Silicates, *Annu. Rev. Mater. Sci.*, 15 (1985) 227-248. <https://doi.org/10.1146/annurev.ms.15.080185.001303>.
- [38] L.M. Hoyos-Palacio, A.G. García, J. F. Pérez-Robles, J. González, H.V. Martínez-Tejada, Catalytic effect of Fe, Ni, Co and Mo on the CNTs production, *IOP Con. Ser. Mater. Sci. Eng.*, 59 (2014) 012005. <https://doi.org/10.1088/1757-899X/59/1/012005>.
- [39] V.M. Irurzun, Y. Tan, D.E. Resasco, Sol-Gel synthesis and characterization of Co-Mo/Silica catalysts for single-walled carbon nanotube production, *Chem. Mater.*, 21 (2009) 2238-2246. <https://doi.org/10.1021/cm900250k>.
- [40] G. Luo, H. Yao, M. Xu, X. Cui, W. Chen, R. Gupta, Z. Xu, Carbon nanotube-silver composite for mercury capture and analysis, *Energy Fuels*, 24 (2010) 419-426. <https://doi.org/10.1021/ef900777v>.
- [41] H. Shir Khanloo, M. Osanloo, M. Ghazaghi, H. Hassani, Validation of a new and cost-effective method for mercury vapor removal based on silver nanoparticles coating on micro glassy balls, *Atmos. Pollut. Res.*, 8 (2017) 359-365. <https://doi.org/10.1016/j.apr.2016.10.004>.
- [42] H. Shir Khanloo, F. Golbabaie, A. Vahid, A. Faghihi Zarandi, A novel nano-palladium embedded on the mesoporous silica nanoparticles for mercury vapor removal from air by the gas field separation consolidation process, *Appl. Nanosci.*, (2022). <https://doi.org/10.1007/s13204-022-02366-0>.
- [43] Y. Ma, T. Xu, X. Zhang, Z. Fei, H. Zhang, H. Xu, Y. Ma, Manganese bridge of mercury and oxygen for elemental mercury capture from industrial flue gas in layered Mn/MCM-22 zeolite, *Fuel*, 283 (2021) 118973. <https://doi.org/10.1016/j.fuel.2020.118973>.
- [44] H. Zhang, J. Wang, T. Liu, M. Zhang, L. Hao, T. Phouthavong, P. Liang, Cu-Zn oxides nanoparticles supported on SBA-15 zeolite as a novel adsorbent for simultaneous removal of H₂S and Hg⁰ in natural gas, *Chem. Eng. J.*, 426 (2021) 131286. <https://doi.org/10.1016/j.cej.2021.131286>.